Scaled Aeroelastic Wind-Tunnel Model Design with Topology Optimization

Bret K. Stanford*

NASA Langley Research Center, Hampton, VA, 23681

The goal of this work is to use numerical topology optimization to design aeroelastically-scaled wind-tunnel flutter models of a generic transport configuration, to be tested in the Transonic Dynamics Tunnel, as part of an envisioned validation experiment for transonic flutter. The topological design dictates the structural details of a variable-thickness aluminum plate located at the midsurface of the outer mold line, in order to satisfy the various conflicting design requirements including a prescribed flutter boundary, flutter frequency, and static stress levels. Four designs are demonstrated in this paper, where it is shown that the inclusion of a cylindrical tip store can help ease the conflict between low stiffness (to allow a wing to flutter in the tunnel envelope) and high strength (to ensure safe structural response). The tip store complicates the geometrical features of the wing, however, and is generally undesirable from the vantage point of a validation experiment. Results from this paper will show that with careful attention to constraint boundary settings and design parameterizations, it is possible to optimize the design of a complex aeroelastic wind-tunnel model primary structure.

I. Introduction

Despite recent advances in computational aeroelasticity, accurate predictions of flutter mechanisms driven by transonic physics (shocked flow, separated flow) remain challenging. These challenges are compounded by the fact that there are relatively few transonic experimental validation data sets available for benchmarking solvers focused on aeroelastic predictions. The most popular two test cases are the AGARD 445.6 test case,[1] and the Benchmark Models Program (BMP),[2] both tested at the NASA LaRC Transonic Dynamics Tunnel. The AGARD 445.6 test case, however, displays very little transonic behavior (i.e., flow nonlinearity), due to the thin airfoil tested at small angles of attack.[3] The BMP is focused on relatively simple wing geometries with rigid structures attached to a pitch-and-plunge apparatus (though the resulting flutter mechanisms do feature rich flow physics). There is a need for additional experimental validation data sets for transonic aeroelastic flutter, that feature relatively realistic structural and geometric configurations, in addition to complex flow physics.

The envisioned requirements for such a model are listed below.

1. A prescribed dynamic pressure flutter boundary as a function of Mach number throughout the TDT envelope, with a well-defined transonic flutter "dip", in addition to a prescribed flutter reduced frequency.
2. A static aeroelastic response within required safety factors, throughout the expected operating region of the tunnel envelope.
3. A simple, monolithic, well-defined outer mold line (OML) with high-quality surface finish.

The final OML requirement is driven by a desire to minimize uncertainties in computation fluid dynamics (CFD) predictions; even simple geometries can invoke strong flow nonlinearities, for sufficiently high Mach numbers and angles of attack (as evidenced by the BMP). However, one consistent hallmark of aeroelastic model design is the use of stores, bodies, pylons, or wing breaks, to lower the torsional frequency of the model and allow for the occurrence of flutter at reasonably low dynamic pressures within the tunnel envelope: see

*Research Aerospace Engineer, Aeroelasticity Branch, AIAA Associate Fellow, bret.k.stanford@nasa.gov.

Ref. 4, for example. The resulting geometry of this segmented wing-body assembly would complicate the numerical benchmarking process, and is to be avoided.

If, then, flutter is to occur at a reasonably-low dynamic pressure without these conventional model design methods, this places the onus on a highly-tuned stiffness and mass distribution inside the OML, in order to obtain the three conflicting requirements listed above. Formal numerical aeroelastic optimization can be used to obtain a design with prescribed flutter dynamic pressures, flutter frequencies, flutter mechanisms, and static aeroelastic response. Previous aeroelastic optimization work in the area of model design is seen in Ref. 5, with a specific focus on maintaining scaling similitude in Refs. 6 and 7.

This work seeks to satisfy the requirements listed above within the jig shape OML of a full-span, sting-mounted Common Research Model (CRM) configuration, to be tested in the TDT. The CRM is a well-known test case for scaled, rigid, wind-tunnel models,[8] as well as for numerical modeling of full-span aeroelastic configurations.[9] This paper will demonstrate a conceptual design exercise of the proposed CRM aeroelastic validation model. Due to the anticipated difficulties in obtaining a structural design that simultaneously meets each of the conflicting requirements listed above, aggressive optimization techniques will be used, including topological design[10] and material design.[11]

II. Aeroelastic Modeling and Optimization

The jig shape used here is based on the CRM, and is taken from Ref. 9 with a geometric scale factor of 0.052 relative to the full-scale model, leaving a wingspan of 10 ft. For the results shown here, however, only a half-span model is considered, with the wing structure fully clamped at the unmodeled wing-body intersection.

The model construction considered here is a layered metallic shell along the camber line of the CRM wing, with foam to preserve the desired jig shape OML (taken from Ref. 9). The layered plate consists of an aluminum core, and a bonded outer shell of tungsten; at every location on the planform, the optimizer may choose the thickness of each material. The lower bound on the thickness of each material is 0.32", though in some locations of the wing, near the leading and trailing edges, the thickness of the OML is less than this lower bound, and so the lower bound is set to 90% of the OML thickness. The optimizer may also choose not to use one or both metals at a given planform location; in this case, the wing is entirely constructed of foam from the upper OML surface to the lower. Otherwise, the optimizer must ensure that the total shell thickness at a given location is no larger than the thickness of the jig OML, in order to preserve the OML shape. An example of this can be seen in Fig. 1, where the airfoil is thin enough towards the trailing edge, that the structure itself serves as the OML rather than the foam.

The objective function for the optimizer is to minimize structural mass, which is used here as a surrogate for manufacturing cost. There are four design variables attached to every finite element: the thickness of the two materials (aluminum and tungsten), and the "topology" of the two materials. The topology space consists of continuous variables between 0 and 1; a value of 1 means that the material is present, and a value of 0 means that it is not. Even if the topology of one or both materials is set to 1 at a given location, foam is still used above and below the layered metallic plate, to form the desired jig OML. If the topology of both materials is set to 0 at a given location, this means that there is a cut-out at that location, with foam used for the entire wing depth from upper to lower surface. As further indicated in Fig. 1, the topology of the base aluminum plate is fixed to 1 (i.e., nondesignable) along the perimeter of the wing planform.

For some optimization cases, a thin aluminum store (rod) was added to the wingtip to facilitate flutter. This idea goes against the design principles outlined above (i.e., a simple single-bodied OML), but was found to be required in order to obtain a reasonable response at higher angles of attack. For these cases, the optimizer, in addition to dictating the stiffness and topological details along the wing structure, also decides on the store geometry: length, diameter, and attachment point.

The optimization constraints are summarized below:

1. A constraint that ensures that the total thickness of the layered metallic plate is not greater than the prescribed wing OML thickness, at every point within the planform.
2. An equality constraint on the flutter dynamic pressure: a flutter dynamic pressure Q_f of 150 psf at Mach number 0.8.
3. An equality constraint on the flutter reduced frequency, k_f. Two separate models are desired, one that flutters at a relatively low reduced frequency in the range of 0.05-0.1 (quasisteady flutter), and one that flutters at a relatively high value in the range of 0.4-0.5 (unsteady flutter).

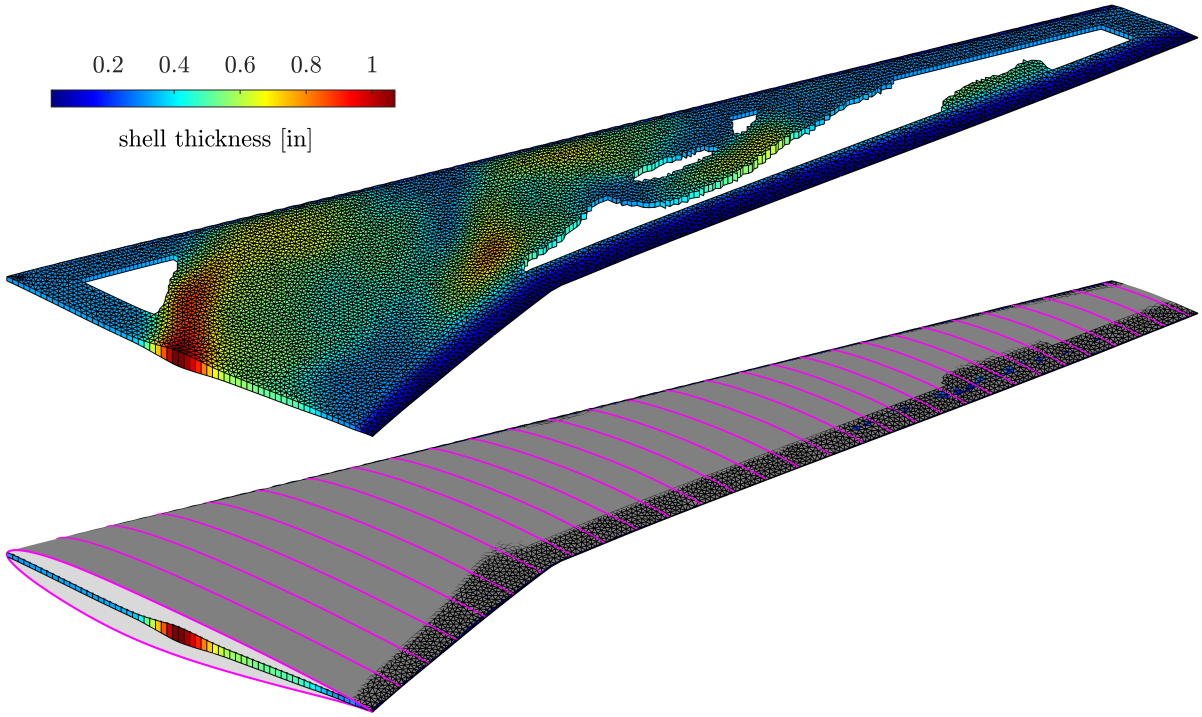


Figure 1: Sample wing structure and foam OML.

4. A static aeroelastic stress constraint at a prescribed Mach, dynamic pressure, and AoA triplet. Von Mises stresses are computed in all 3 materials (aluminum, tungsten, foam), aggregated into a single stress metric for each material, and enforced to a safety factor of four. This constraint is implemented at a Q value of 300 psf, Mach 0.8, and AoA values between 3° and 5°.
5. A dynamic aeroelastic stress constraint: oscillatory fluttering motion is scaled to a prescribed amplitude, and superimposed upon static aeroelastic deformations obtained at the flutter point. Time-dependent aggregated von Mises stresses from this procedure are again enforced to a safety factor of four.

Linear aeroelastic tools are utilized to compute static and dynamic aeroelastic behavior: a coupling of a linear shell/plate finite element structural dynamic model to the doublet lattice method unsteady aerodynamic tool. Such a tool is incapable of predicting the transonic flutter dip mechanisms[12] of interest here, but the expectation is that the linear flutter mechanism will be moderately similar to the nonlinear CFD-based flutter mechanism computed near zero-lift. Stronger lifting flows at higher AoA will exacerbate the nonlinearities, and lead to the flutter dips of interest. The static aeroelastic stress constraint has been located at a higher Q and AoA value, in order to safely observe the recovery-side ("back-side") of the flutter dip, though high-strength requirements needed to satisfy the static stress constraints directly conflict with low-stiffness requirements needed for the model to flutter at lower Q-values. The addition of the tip store can help ease this design conflict, as the tip store helps maintain low flutter Q values without reducing stiffness.

As noted, two separate models are sought here: one which flutters at a low frequency, and another which flutters at a high frequency. This provides an interesting dichotomy in the role of unsteady aerodynamics, where the model with the low k_f exhibits a quasisteady flutter mechanism.

The final constraint listed above is meant to provide some means of including a flutter observability metric, to understand how much deflection can be withstood at a flutter condition before a certain safety factor is lost. The ability to satisfy this constraint is entirely dependent on the chosen flutter amplitude, and it is difficult to quantify this metric. The peak flutter amplitude observed during a test would depend on (1) what sort of disturbance pushes the design from a stable Q to the current unstable Q, (2), how far the current unstable Q is above the flutter point Q_f, and (3) how much time elapses in the unstable condition before the condition is reduced rapidly by manually triggering the TDT bypass valves (i.e., reaction time).

Rather than trying to quantify each of those metrics, the dynamic flutter constraint in this work is evaluated at a fixed flutter amplitude of 1", and as will be seen, only the low-frequency designs are able to honor this constraint.

III. Results

Optimal results are shown for four designs in Figure 2, in terms of optimal thickness distributions, topologies, and (if using) store geometry. Structural thickness is indicated by the color contours; areas along the wing where a layer of tungsten is used to reinforce the aluminum plate, are outlined with a magenta curve. These four designs are summarized as:

- Design A: a low-frequency design ($k_f = 0.099$) without a tip store, which flutters very close to the required flutter Q of 150 psf. The stress-based safety factor of four can be maintained up to an AoA of 3°, when the Mach number is 0.8 and the dynamic pressure is 300 psf. If the AoA is set higher than 3°, the design process no longer closes, as noted previously. This design features diagonally-oriented members between the leading and trailing edge spars, in an effort to reduce torsional stiffness (and allow for flutter) while maintaining a certain level of bending stiffness (for high strength).
- Design B: a second low-frequency design, but now including a tip store. The inclusion of this store (designed to a long, thin profile, and attached to the wing at the store's leading edge) allows this design to be statically tested to a higher AoA of 5°. This design shares topological similarities with design A, but the diagonal members extend all the way to the wing root.
- Design C: a high-frequency design ($k_f = 0.448$) without a tip store, capable of maintaining the required safety factor up through 4° AoA. This design involves a central spar-like member, disconnected from the leading and trailing spars, and attached to a large section of tungsten at the root of the member. This design is not able to satisfy the 1" dynamic stress constraint: including this constraint in the design process precludes the design from properly closing.
- Design D: a second high-frequency design, but now including a tip store. Unlike design B, this store is very short, with a large diameter, and is attached to the wing at the store's trailing edge. The inclusion of the store allows only one additional degree of tested AoA (up to 5°), leading to the conclusion that the addition of a tip store is not as critical for these high-frequency designs. Like design C, this design is not able to satisfy the 1" dynamic stress constraint.

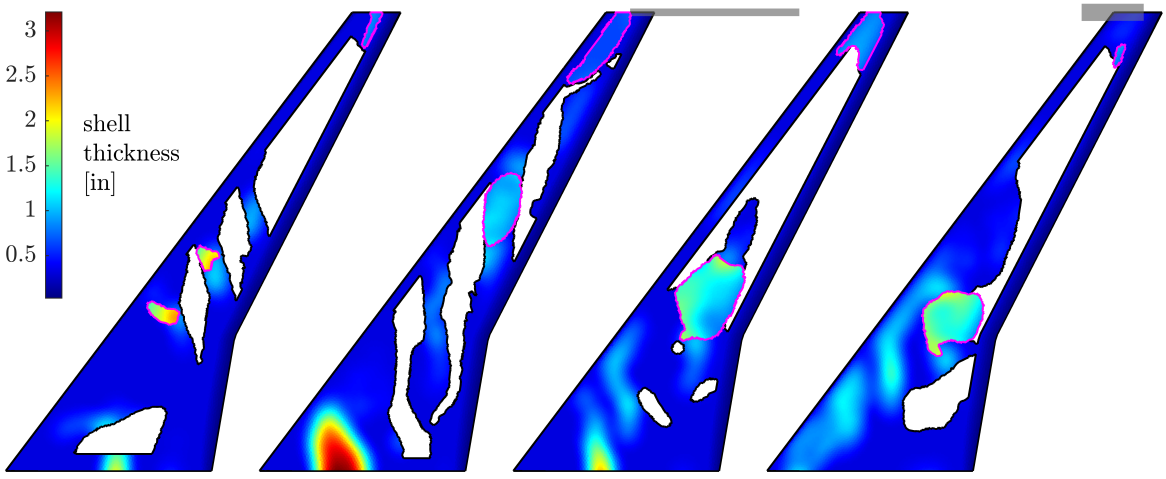


Figure 2: Optimal wing thickness and topologies: areas of tungsten are indicated with a magenta outline.

The static aeroelastic deflections and subsequent von Mises stresses (normalized by the yield stress) are shown in Figure 3, for each of the four designs. Stresses are shown for the aluminum layer only. Safety

factors are given as the inverse of the contoured values in Figure 3: for example, a safety factor of four is maintained wherever the normalized von Mises stresses are below 0.25. The peak normalized von Mises stress found along the wing is further quantified in Figure 4 as a function of dynamic pressure at 5°; this figure also plots the tip displacement at these same conditions, normalized by the semispan length.

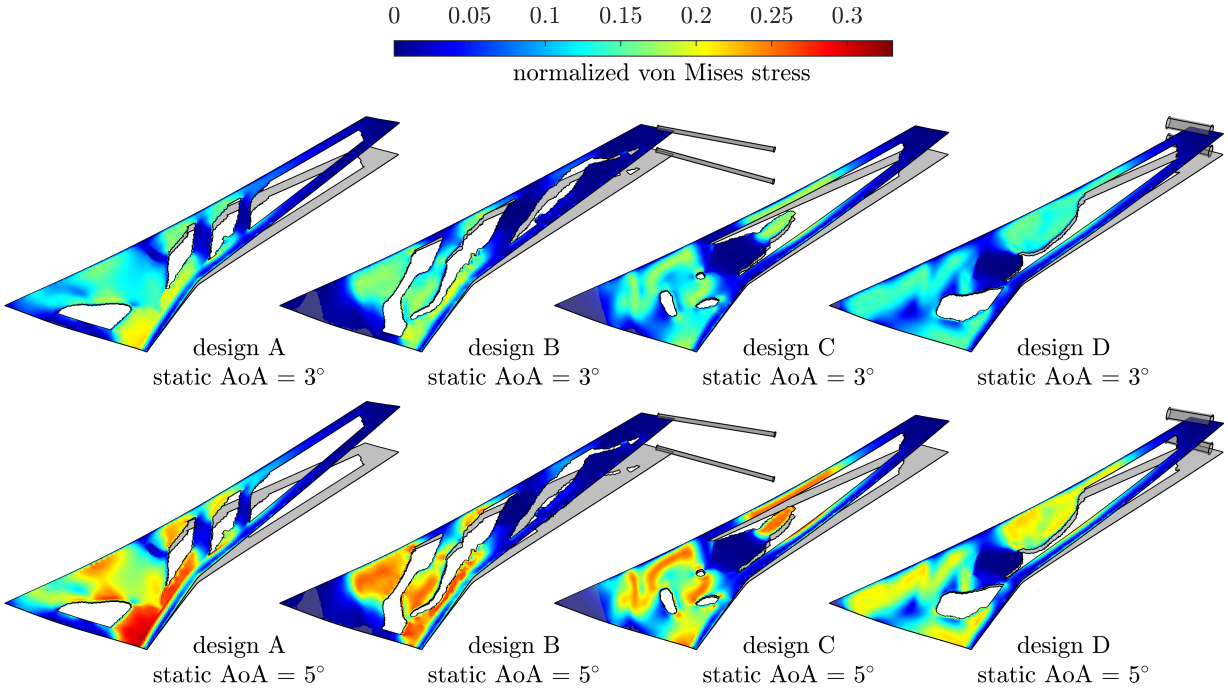


Figure 3: Static aeroelastic response at 3° (top row) and 5° (bottom row) AoA for each of the 4 designs at 300 psf.

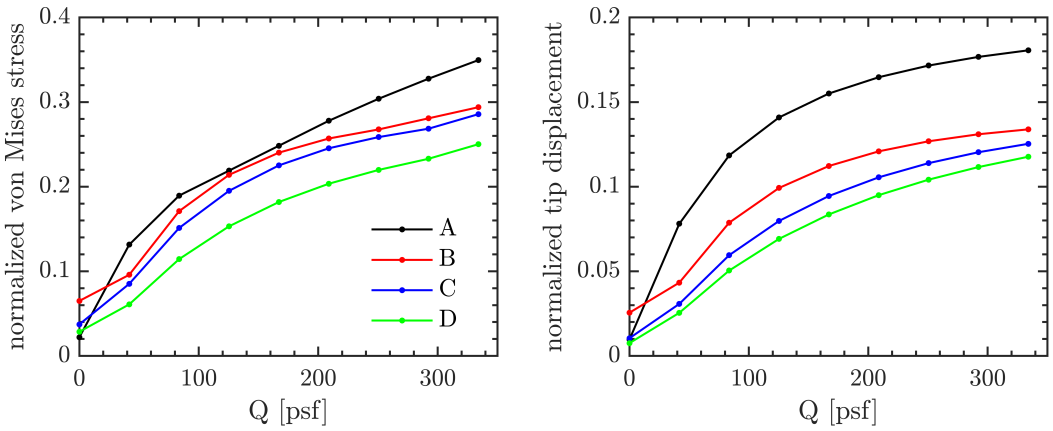


Figure 4: Static aeroelastic response as a function of dynamic pressure Q, at 5° AoA for each of the 4 designs.

Referencing Figure 3, each design maintains the safety factor of four at 3° AoA and 5° AoA at 300 psf, with the exception of design A, which is only designed up to an AoA of 3°, as noted above. Deflections are on the order of 10-15% (again with the exception of design A, which deflects more), which is a value likely within the range of validity for the linear finite element model used here. These bending deflections decrease the sectional lift relative to a rigid wing (as shown in Figure 5) due to the fact that the wing is swept; the low-frequency designs A and B display some additional torsion relative to the high-frequency designs C and D, as evidenced by the decreased lift along the span. This loss of lift may blunt the severity of the transonic flutter dip eventually noted for these designs, since the flow nonlinearities at the tip will be weakened by the large amounts of washout.

Lastly, it is noted that the peak stresses in Figure 3 are not relegated to a few locations on the structure, but are instead spread out over large portions of the plate, particularly for designs B, C, and D. This is a natural by-product of the structural optimization process used here, which seeks to minimize mass under (among other constraints) a stress constraint: a "fully-stressed design".

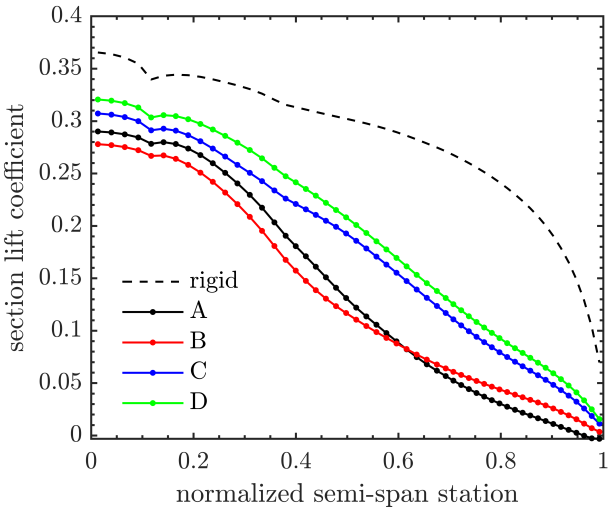


Figure 5: Sectional lift distribution at 5° AoA, 300 psf, compared with the lift of the rigid wing.

Next, eigenvalue migration plots are shown in Figure 6 for each of the four designs. The low-frequency designs show strong coupling of modes 1 (first bending) and 2 (second bending with some torsion), leading to an instability of mode 1. The high-frequency designs show strong coupling of modes 3 and 4, two modes which are characterized by outboard bending and torsion. These plots mostly conform to the Q_f and k_f specifications listed above, but several potential concerns are noted. First, designs A and C display a secondary flutter mechanism: design A, for example, shows the primary sought-after flutter mode as a coupling of modes 1 and 2, but the 3/4 coupling is evident also, though this flutter mechanism exists above 400 psf. Competing flutter modes could be problematic for testing, given the modeling uncertainties encountered here, and the possibility that the sought-after flutter mode may not, once tested, actually be the critical flutter mode observed in the tunnel. Second, the unstable damping for each case may be relatively low, as the crossing of the real eigenvalue part from negative to positive is relatively shallow. Higher (steeper) slopes are perhaps desirable from a numerical modeling perspective, since they are less susceptible to numerical uncertainties. Alternatively, shallower slopes allow for greater and safer observability of the flutter mechanisms, a metric that will be discussed in more detail below. Finally, the dimensional flutter frequency of designs C and D is fairly large, between 40 and 50 Hz. These high frequencies will lead to further observability challenges during the testing process, but cannot be avoided if a reduced frequency k_f is desired in the range of 0.4-0.5 at these model scales.

Finally, dynamic aeroelastic stresses are shown in Figures 7 -10, for the four designs. This process involves computing the static aeroelastic deflections at the flutter point of each design (additionally at 5° AoA), and then superimposing an oscillating flutter mode at a prescribed amplitude. Each figure shows results from amplitudes (as measured by maximum structural displacement) of 0.5", 1", 2", and 3", in terms of phase-plane plots of normalized von Mises stresses versus the structural deflection, where dynamic stress is computed with a modal acceleration (MA) method.[13] The contour plots on the right of each figure shows the structural response for the minimum and maximum structural deflection for the 3" amplitude case.

As noted, the low-frequency designs A and B are designed to a safety factor of four up to a dynamic amplitude of 1", and this constraint is only slightly violated in Figure 7 and 8. Up to an amplitude of 3", design A shows a peak normalized stress of 0.35 (safety factor = 2.86) and design B a peak stress of 0.42 (safety factor = 2.38). Design A, at all amplitudes, shows a clear break in the phase-plane plot, where the location of the critical stress along the wing changes: at minimum deflections, the peak stress is near the root (which largely corresponds to the peak stress profile of the static deflections). At higher deflections,

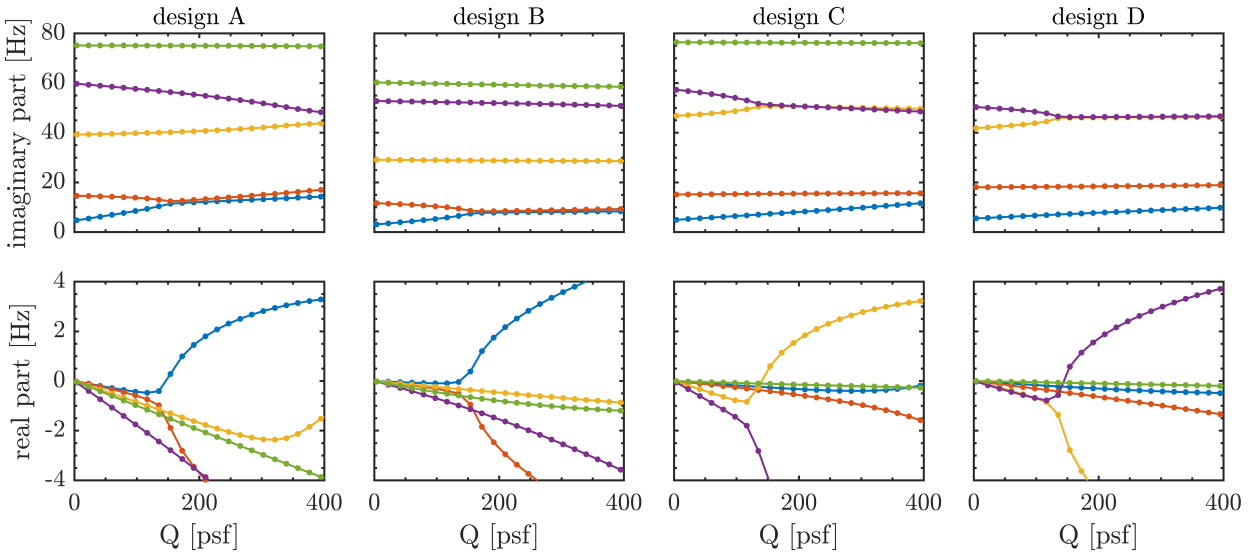


Figure 6: Dynamic aeroelastic eigenvalue migration plots for each design.

the inertial loading pushes the peak stresses out towards the wing tip. For design B, the phase-plane plot is continuous, and also free of hysteresis.

For the high-frequency designs C and D, the optimization is not able to accommodate the 1" dynamic stress constraint, and so these two designs are simply post-processed for this metric. Stresses for these two designs are largest outboard, at the leading and trailing spar structures. At 1" of deflection, the safety factors are 2.08 (design C) and 2.22 (design D), but both designs experience elastic failure for 3" deflections. At larger deflections, the presence of the tip store generally exacerbates the dynamic stresses, though the connection between the wing and the store is idealized in this work, with rigid body connections.

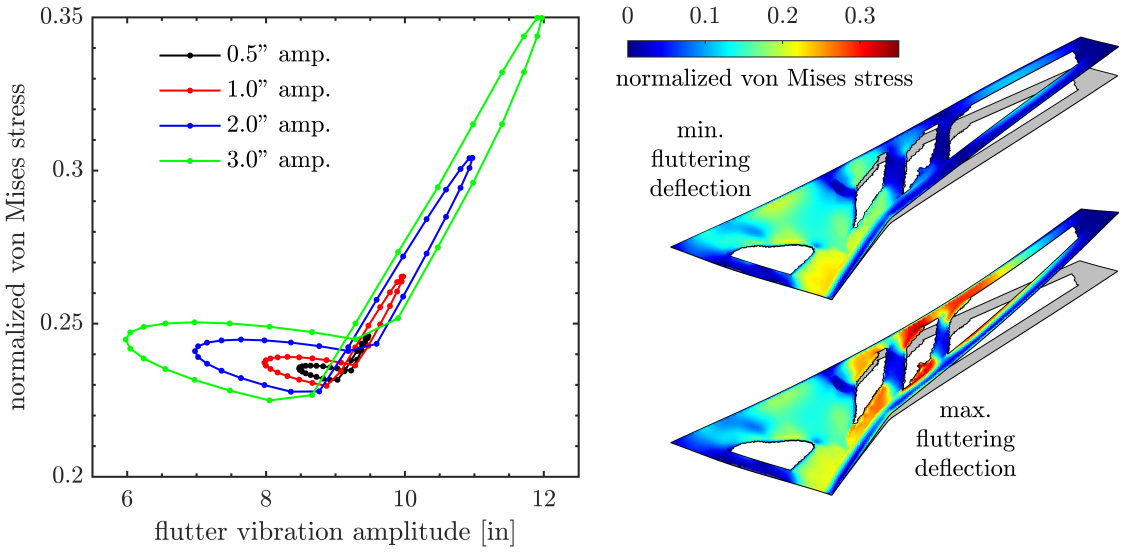


Figure 7: Dynamic aeroelastic stress behavior at the flutter point for design A.

IV. Conclusions

Topology optimization studies have been presented for the design of an aeroelastic model to be tested in the Transonic Dynamics Tunnel (TDT). This model is patterned off of the Common Research Model (CRM),

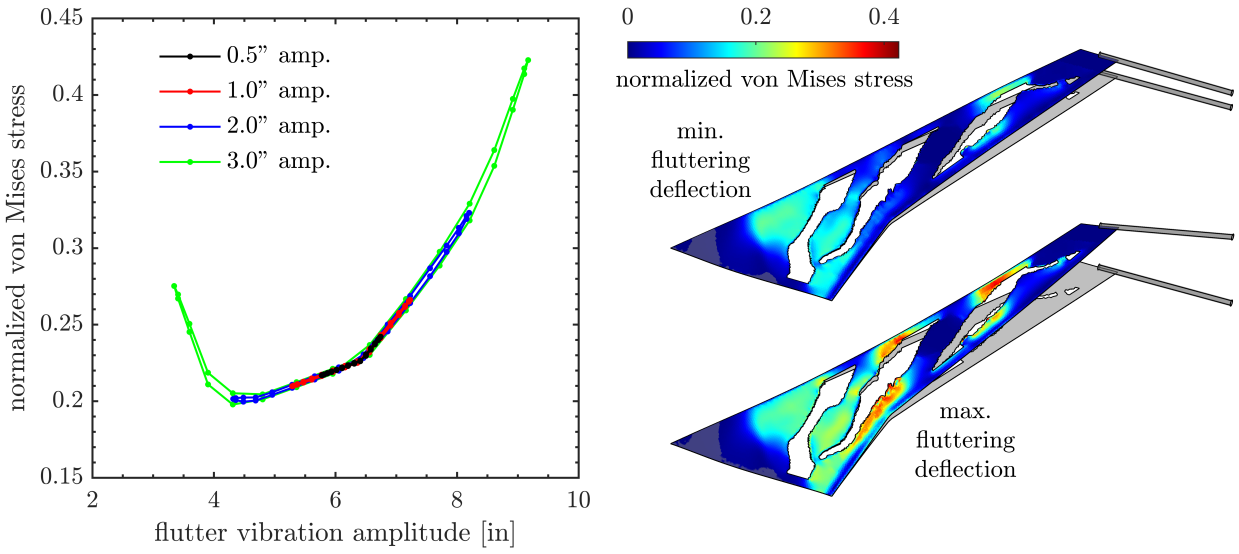


Figure 8: Dynamic aeroelastic stress behavior at the flutter point for design B.

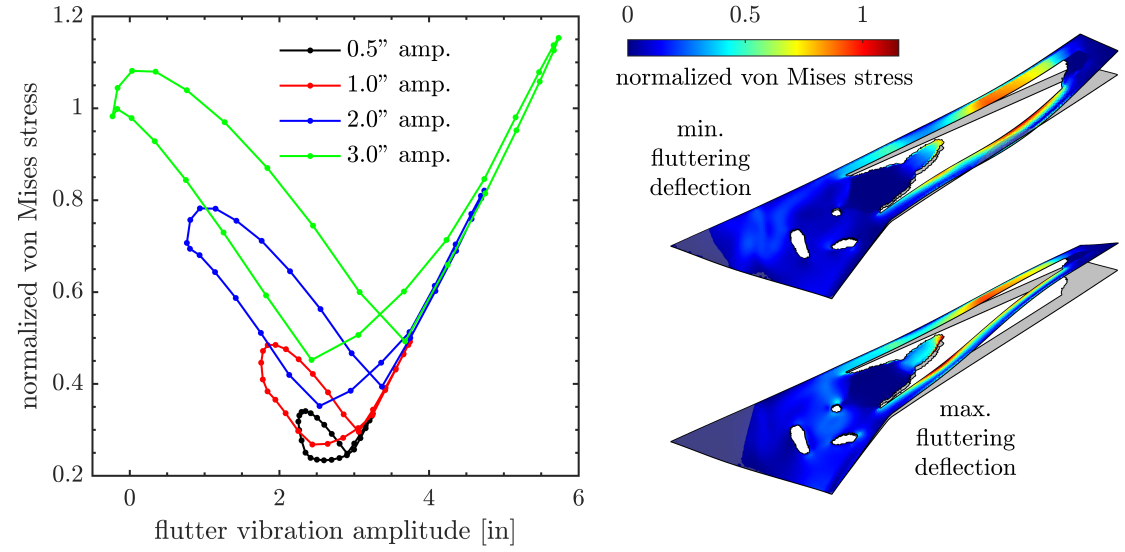


Figure 9: Dynamic aeroelastic stress behavior at the flutter point for design C.

where the internal structure of the wing is optimized to produce the desired aeroelastic metrics. The test is specifically envisioned as a validation test for CFD predictions of transonic flutter. The design of such models is difficult, governed by a strong conflict between low stiffness (such that the model flutters within the tunnel envelope) and high strength (to ensure a safe structural response). The design space afforded by topological design schemes helps to provide a closed design, which can satisfy the competing objectives.

Four designs are presented here: wings designed to flutter at low and high flutter frequencies, with and without the use of a tip store. The use of a tip store (whose geometry is designed by the numerical optimizer) is not ideal, as it complicates the outer mold line of the wing geometry and would further complicate the CFD validation process. On the other hand, a tip store can help the wing flutter within the envelope without the need to decrease stiffness, which eases the conflict against the high-strength requirements. Specifically, the use of tip store can enable a design which is cleared to test at higher angles of attack and dynamic pressures, though this is found to be more useful for designs that flutter at lower frequencies, as opposed to

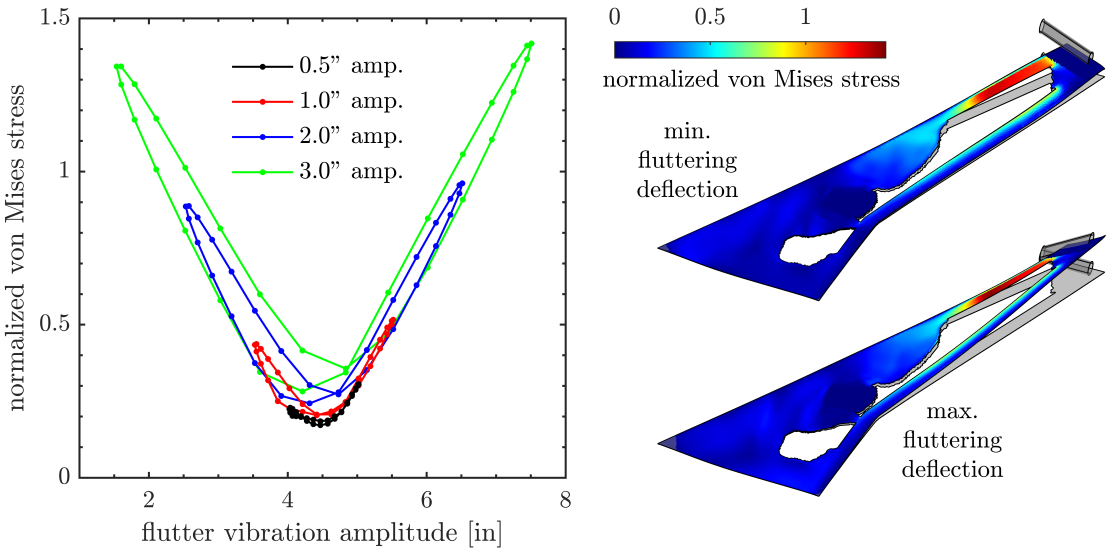


Figure 10: Dynamic aeroelastic stress behavior at the flutter point for design D.

higher values. Testing at higher angles of attack and dynamic pressures will be useful for transonic flutter behavior, where the recovery-side of the flutter dip can rise to relatively high values.

Each design is further analyzed for dynamic fluttering stress, in an attempt to quantify flutter observability. This process involves computing static aeroelastic deformations at the flutter point, and then superimposing the oscillating flutter mode shape at some prescribed amplitude. With this process, the low-frequency design maintains a safety factor greater than two for flutter amplitudes up to 3". The high-frequency designs, on the other hand, show a safety factor less than one (i.e., failure) for this same flutter amplitude.

Acknowledgments

This work is supported by the Transformational Tools and Technologies (TTT) project of the NASA Transformative Aeronautics Concepts Program (TACP).

References

[1]Yates, C., "AGARD Standard Aeroelastic Configurations for Dynamic Response. Candidate Configuration I - Wing 445.6," NASA TM-100492, August,1987.

[2]Bennett, R., "Test Cases for Flutter of the Benchmark Models Rectangular Wings on the Pitch and Plunge Apparatus," Defense Technical Information Center TR ADPO10713, Fort Belvoir, VA, 2000.

[3]Silva, W., Chwalowski, P., Boyd, P., "Evaluation of Linear, Inviscid, Viscous, and Reduced-Order Modeling Aeroelastic Solutions of the AGARD 445.6 Wing using Root Locus Analysis" *International Journal of Computational Fluid Dynamics*, Vol. 28, No. 3, pp. 122-139, 2014.

[4]Stenfelt, G., Ringertz, U., "Design and Construction of Aeroelastic Wind Tunnel Models," *The Aeronautical Journal*, Vol. 119, No. 1222, pp. 1585-1599, 2015.

[5]French, M., Eastep, F., "Aeroelastic Model Design Using Parameter Identification," *Journal of Aircraft*, Vol. 33, No. 1, pp. 198-202, 1996.

[6]Ricciardi, A,. Canfield, R., Patil, M., Lindsley, N., "Nonlinear Aeroelastic Scaled-Model Design," *Journal of Aircraft*, Vol. 53, No. 1, pp. 20-32, 2016.

[7]Spada, C., Afonso, F., Lau, F., Suleman, A., "Nonlinear Aeroelastic Scaling of High Aspect-Ratio Wings," *Aerospace Science and Technology*, Vol. 63, No. 1, pp. 363-371, 2017.

[8]Rivers, M., Dittberner, A., "Experimental Investigations of the NASA Common Research Model," *Journal of Aircraft*, Vol. 51, No. 4, pp. 1183-1193, 2014.

[9]Brooks, T., Kenway, G., Martins, J., "Benchmark Aerostructural Models for the Study of Transonic Aircraft Wings," *AIAA Journal*, Vol. 56, No. 7, pp. 2840-2855, 2018.

[10]Dunning, P., Stanford, B., Kim, H., "Coupled Aerostructural Topology Optimization using a Level Set Method for 3D Aircraft Wings," *Structural and Multidisciplinary Optimization*, Vol. 51, No. 1, pp. 1113-1132, 2015.

[11]Hvejsel, C., Lund, E., "Material Interpolation Schemes for Unified Topology and Multi-Material Optimization," *Structural and Multidisciplinary Optimization*, Vol. 43, No. 1, pp. 811-825, 2011.

[12]Edwards, J., "Calculated Viscous and Scale Effects on Transonic Aeroelasticity," *Journal of Aircraft*, Vol. 45, No. 6, pp. 1863-1871, 2008.

[13]Blelloch, P., "Calculation of Structural Dynamic Forces and Stresses using Mode Acceleration," *AIAA Journal*, Vol. 12, No. 5, pp. 760-762, 1988.